Electroproduction experiments

1972 J. Phys. A: Gen. Phys. 5 1

(http://iopscience.iop.org/0022-3689/5/1/009)

J. Phys. A: Gen. Phys., Vol. 5, January 1972. Printed in Great Britain

Electroproduction experiments†

F W BRASSE

Deutsches Elektronen-Synchrotron DESY, Hamburg, Germany

MS received 7 June 1971

Abstract. A survey is given for recent experiments in electroproduction and a discussion of their results. For the resonance region the main results are that the ratio of longitudinal to transverse excitation is about as small as it was found for the deep inelastic continuum (about 0·2 or smaller). The excitation of the $\Delta(1236)$ in the π^0 channel, as measured by coincidence techniques, is going mainly through M_{1+}. However, other small contributions like S_{1+} and E_{1+} for the resonant part and E_{0+} and M_{1-} for the nonresonant part are not negligible.

In the deep inelastic region coincidence measurements are reported. Single positive pion production on hydrogen shows a large longitudinal cross section, which can be explained quite well by vector meson dominance. Proton momentum spectra in the direction of the virtual photon do not show an unusually large flux of protons with high momenta as was expected from a specific parton model.

1. Introduction

Experiments on electroproduction have become a very interesting tool to study the structure of the nucleons and their excited states. The field is already so large, that it is impossible to cover everything in a single review. I shall therefore confine myself to recent results on the following subjects:

I. Resonance region
   1. σ_L/σ_T at $\Delta(1236)$
   2. $e+P \rightarrow \underline{e}+\Delta(1236)$
      $\rightarrow \underline{P}+\pi^0$
   3. σ_L/σ_T for higher resonances

II. Deep inelastic region
   1. P and π^+ spectra in the forward direction
   2. Single π^+ production

First let me outline briefly the relevant kinematics. We are interested in the following processes:

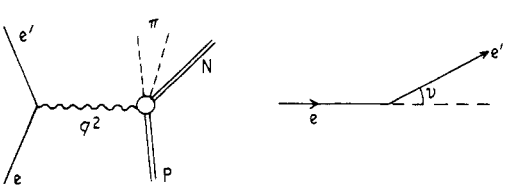

† Talk presented at the Conference on Elementary Particle Physics, Lancaster, England, April 1971.

$q^2 = |\boldsymbol{q}|^2 - q_0^2 = 4EE' \sin^2 \theta/2$ is the four-momentum squared, positive in the spacelike region

$W = \sqrt{s_0}$ the mass of the outgoing hadronic system
$E_\gamma = K = (W^2 - M^2)/2M$ the equivalent photon energy
$\nu = E - E'$ the energy loss of the electron
$\omega = 2M\nu/q^2$ the scaling variable
$\epsilon = \{1 + 2(|\boldsymbol{q}|^2/q^2) \tan^2(\theta/2)\}^{-1}$ the degree of polarization of the virtual photon
$\Gamma = \alpha/2\pi^2 \{E'K/Eq^2(1-\epsilon)\}$.

Then the cross section, if one detects only the scattered electron, can be written in the following way:

$$\frac{d^2\sigma}{d\Omega_e\, dE'} = \Gamma \Sigma \qquad \text{with} \qquad \Sigma = \sigma_T + \epsilon\sigma_L.$$

σ_T and σ_L are the photoabsorption cross sections for transverse and longitudinal photons. They can also be expressed in terms of the structure functions W_1 and W_2:

$$W_1 = \frac{K}{4\pi^2\alpha}\sigma_T$$

$$W_2 = \frac{Kq^2}{4\pi^2\alpha|\boldsymbol{q}|^2}(\sigma_T + \sigma_L).$$

In order to separate σ_L from σ_T one needs measurements of Σ for two different values of ϵ or different scattering angles, but the same values of q^2 and W. For coincidence measurements on a specific final state such as single pion production, the cross section can be written, again in the one-photon exchange approximation

$$\frac{d^3\sigma}{d\Omega_e\, dE'\, d\Omega^*} = \Gamma \frac{d\rho}{d\Omega^*}$$

$$\frac{d\sigma}{d\Omega^*} = A + \epsilon B + \epsilon C \sin^2\theta^* \cos 2\phi + \{\epsilon(1+\epsilon)\}^{1/2} D \sin\theta^* \cos\phi.$$

θ^* and ϕ are the polar and azimuthal angles of the outgoing π in the π, N rest system. The coefficients of the angular distribution are functions of q^2, W and $\cos\theta^*$. The terms are the cross sections for unpolarized transverse photons A, for longitudinal B and polarized transverse photons C, and the interference between transverse and longitudinal photons D. Since there are no results where ϵ has been varied, I will use the sum

$$\bar{A} = A + \epsilon B.$$

If one assumes for the production of the $\Delta(1236)$ resonance that only s and p waves contribute, the coefficients can be evaluated with respect to θ^* as follows:

$$\bar{A} = \bar{A}_0 + \bar{A}_1 \cos\theta^* + \bar{A}_2 \cos^2\theta^*$$

$$C = C_0$$

$$D = D_0 + D_1 \cos\theta^*.$$

The new coefficients are now only functions of q^2 and W. There are six of these to be determined. These again can be evaluated in terms of the multipole amplitudes E_{0+}, M_{1-}, M_{1+}, E_{1+}, S_{0+}, S_{1-} and S_{1+}. With real and imaginary parts of these one would have to determine 14 parameters, which is quite impossible to do. In addition they would still be mixtures of different isospin states. One has therefore to make assumptions, if one wants to determine the main multipole amplitudes. I will come back to this later.

2. Resonance region

2.1. σ_L/σ_T *at* $\Delta(1236)$

I can now start discussing experiments. Firstly, in the *region of the first nucleon resonance*, the $\Delta(1236)$, there are new single arm measurements to determine transverse and longitudinal parts of the cross section $\sigma_T + \epsilon\sigma_L$, by two groups: Bartel *et al* (1971) at DESY and Bätzner *et al* (1971) at Bonn.

About three years ago Bartel *et al* (1968) had made measurements at small scattering angles or large values of ϵ and had combined their measurements with those from other groups (Lynch *et al* 1967, Brasse *et al* 1968), at small values of ϵ, to separate σ_L from σ_T. The result at the resonance was a nonzero σ_L below $q^2 = 0{\cdot}5$ GeV^2. This group has now made new large-angle measurements at 86°, using a focusing magnetic spectrometer with a large acceptance. They have checked its acceptance very carefully with respect to the old small-angle spectrometer by elastic scattering so that, at least for the ratio σ_L/σ_T, normalization errors are minimized. Their results are shown in figure 1, where σ_L and σ_T are plotted as a function of W for different ranges of q^2. σ_L is almost everywhere compatible with zero within the error bars but it may have at resonance about 10% of σ_T. The curves are the result of the theoretical dispersion calculations of Gutbrod and Simon (1967). For the longitudinal part, however, these authors believe that their results are not reliable.

The other group has made a few new sets of measurements at $q^2 = 0{\cdot}3$ GeV^2 using the same spectrometer for small and large angles. Their result at $W = 1{\cdot}22$ GeV is shown, together with those from Bartel *et al*, in figure 2. Here the ratio σ_L/σ_T is plotted against the momentum transfer q^2. Also shown are the old results. At $q^2 = 0{\cdot}78$ GeV the new result agrees with the old combination between Bartel *et al* and the group of my colleagues. The discrepancy is with respect to the combination Bartel *et al* with Lynch *et al*. From the new results one may conclude that $R < 0{\cdot}15$.

2.2. Coincidence measurements at $\Delta(1236)$

I will turn now to the *coincidence measurements* at the $\Delta(1236)$ in the π^0 channel:

$$e + p \rightarrow \underline{e} + \underline{p} + \pi^0$$

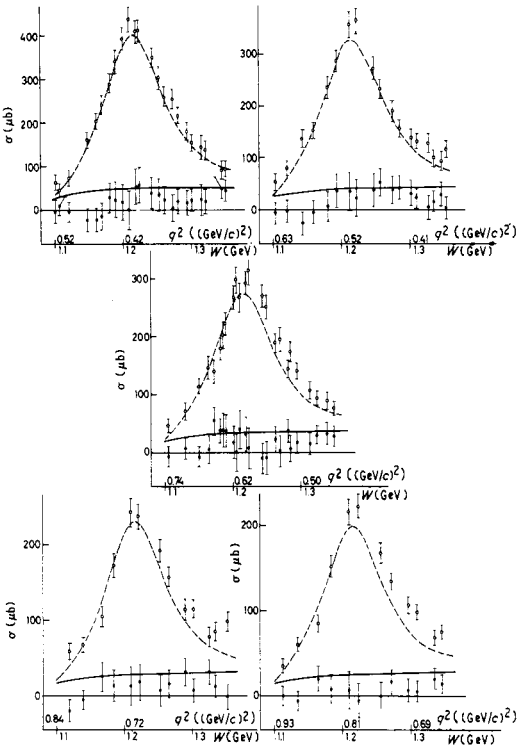

Figure 1. σ_T (open circles) and σ_L (full circles) in the region of the first resonance as measured by Bartel *et al* (1971).

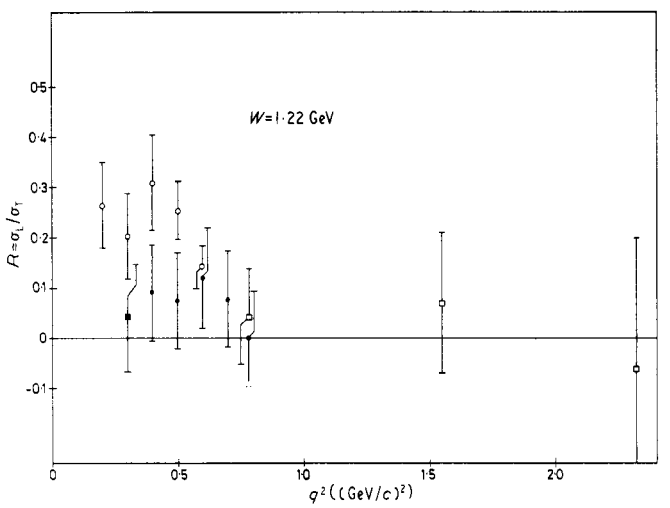

Figure 2. The ratio $R = \sigma_L/\sigma_T$ as function of the momentum transfer q^2 at the first resonance. ⁞ Bartel *et al* (1968, 1971); ⁞ Bätzner *et al* (1971); ⁞ Bartel *et al* (1968) and Lynch *et al* (1967); ⁞ Bartel *et al* (1968) and Brasse *et al* (1967).

where the electron and proton have been detected in coincidence. There are now results from four groups, giving almost complete angular distributions:

(i) Mistretta *et al* (1969), CEA, 1968
at mainly $q^2 = 0{\cdot}25\ \mathrm{GeV}^2$
(ii) Moritz *et al* (1970, 1971), Karlsruhe/DESY
at $q^2 = 0{\cdot}35, 1{\cdot}0\ \mathrm{GeV}^2$
(iii) Hellings *et al* (1971), Manchester/Lancaster
at $q^2 = 0{\cdot}3, 0{\cdot}45, 0{\cdot}6, 0{\cdot}76\ \mathrm{GeV}^2$
(iv) Albrecht *et al* (1970, 1971), DESY/Coll. de France
at $q^2 = 0{\cdot}58, 0{\cdot}98, (1{\cdot}56)\ \mathrm{GeV}^2$.

Their results cover together at the moment the range in q^2 from 0·2 to 1·0 GeV^2.

The last two groups used magnetic spectrometers for the detection of both charged particles with complete determination of the variables of both particles. Therefore they could determine the missing mass and separate out inelastic events and reduce background. In addition the forward cone of the protons could be easily separated from the backward cone; the resolution in θ^* was about 5 to 10°. The other groups used for the proton only hodoscopes and no magnetic field (except for a weak clearing field in the CEA experiment). To illustrate this, the apparatus of the Karlsruhe group is shown in figure 3. The electron is detected in a magnetic nonfocusing spectrometer with vertical bending and wire spark chambers to determine the trajectories. The electron is identified by a shower and Čerenkov counter. This spectrometer turned out to be a very useful instrument. It has a large momentum acceptance reaching from elastic scattering across two resonances with good resolution. The proton angles are measured in a hodoscope of 12×12 scintillators with 2·50° bin size. The protons are separated from lighter particles by $\mathrm{d}E/\mathrm{d}x$ counters (five centimetres thick). The size of the hodoscope is such that, at least at $q^2 = 1\ \mathrm{GeV}^2$, the full decay cone could be accepted. But the resolution in θ^* is much worse than if one uses a magnetic field. On the other hand, variation of the cross section with respect to the azimuthal angle ϕ should be recognized very easily.

As a typical example for the method of data handling in the experiment of the DESY/Collège de France collaboration I would like to show the following missing mass distributions (figure 4). In the upper half the distribution of events against the square of the missing mass is shown for two different values of the total hadronic outgoing mass W, namely 1·216 and 1·256 GeV. With increasing W the possible range for the pion missing mass increases also, leading to a wider distribution. In addition, at 1·256 GeV, two-pion production contributes already. In the lower part we see the same distribution for Monte Carlo events. We have tried to simulate the experiment as far as possible, including all effects like radiation, multiple scattering, randoms and so on. For the calculation of cross sections, equal cuts were then made on both the experimental and the Monte Carlo events as for example to take out badly defined events.

I shall compare now the results of the different laboratories in terms of the six coefficients of the angular distribution. In figure 5 the results of the CEA group at $q^2 = 0{\cdot}25\ \mathrm{GeV}^2$ are plotted together with those for photoproduction as a function of the resonance energy W. The photoproduction data are from the Bonn group (Fischer *et al* 1970). In the case of unpolarized real photons we only have the three coefficients A_0, A_1 and A_2. For a pure M_{1+} transition, $\bar{A}_0/\bar{A}_2$ should be 5/3 and $\bar{A}_2 = C_0$, whereas the other coefficients should be zero. At the resonant energy in photoproduction these relations are quite well fulfilled. However, A_1 only goes through zero there, indicating

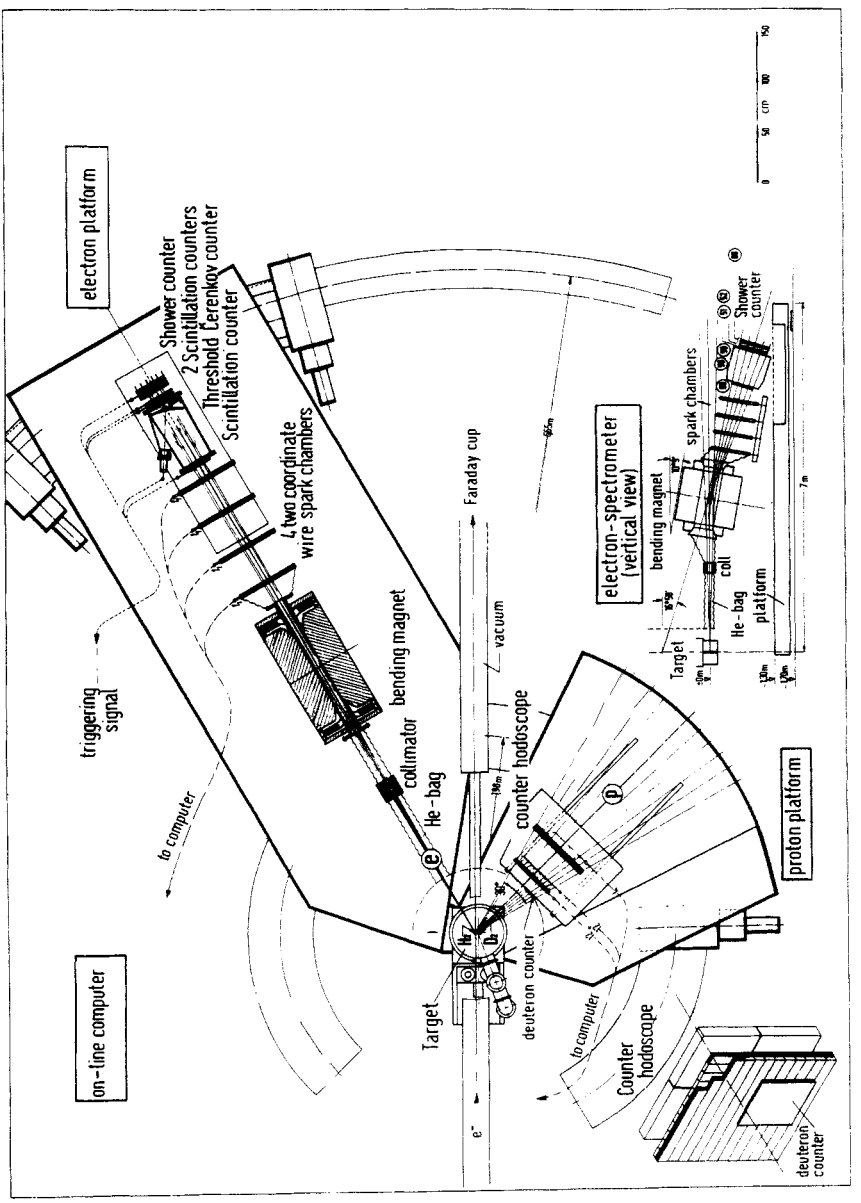

Figure 3. The apparatus used by the Karlsruhe group (Moritz *et al* 1970) for coincidence measurements between the electron and proton at the first resonance.

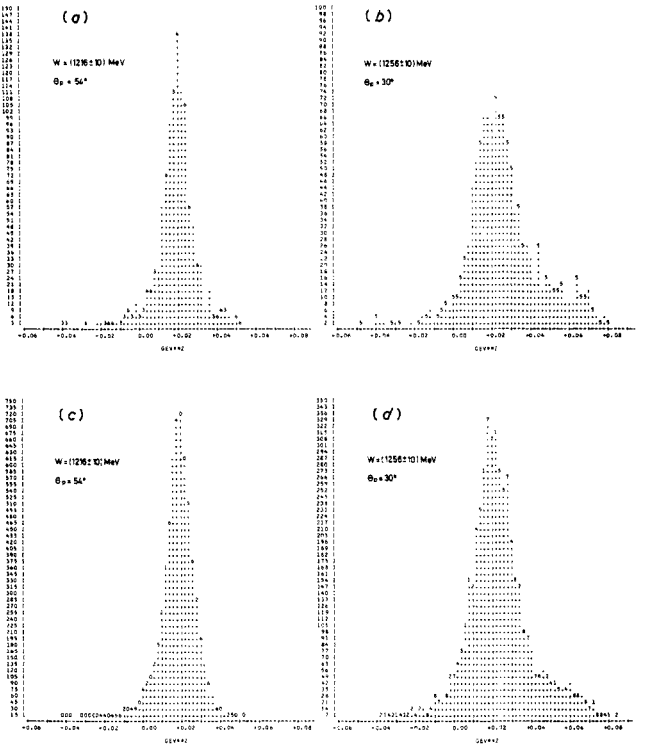

Figure 4. Missing mass distributions of the proton, measured in coincidence with the electron, (*a*), (*b*) for the experiment and (*c*), (*d*) for the simulation by Monte Carlo of the DESY/Collège de France group (Albrecht *et al* 1970).

very nicely the interference between a resonant p wave and a nonresonant s wave. For $q^2 = 0{\cdot}25\,\mathrm{GeV}^2$, $\bar{A}_0$ and $\bar{A}_2$ are not very different from those in photoproduction ($\bar{A}_0$ about $30\,\mu\mathrm{b\,sr}^{-1}$) except on the high mass side of the resonance. $\bar{A}_2$ and C_0 are not equal, indicating also a deviation from a pure M_{1+} transition. D_1 shows that there are small scalar components interfering with the transverse only. Because of their incomplete angular distribution ($\theta^* > 100°$ only, the backward proton being stopped before reaching the hodoscope) and because of the θ^* resolution they could not determine $\bar{A}_1$ nor could they separate D_0 and D_1. They therefore set A_1 and D_0 to zero, the latter assumption being because the dependence on W indicated interference between resonant transverse and longitudinal amplitudes.

At a higher momentum transfer (figure 6) we have results from Karlsruhe at $q^2 = 0{\cdot}35\,\mathrm{GeV}^2$ and from the Lancaster–Manchester collaboration at $q^2 = 0{\cdot}45\,\mathrm{GeV}^2$. For the Karlsruhe group there are similar difficulties as for the CEA group for reasons which I discussed earlier. They could not isolate terms proportional to $\cos\theta^*$, so they set D_1 and $\bar{A}_1$ to zero, hoping that forward and backward parts cancel each other, and in addition they set D_0 to zero, but here allowing the fit to give errors. It may therefore not be too surprising that we see for $\bar{A}_0$, $\bar{A}_2$ and C_0 large differences between the two measurements, especially in view of the fact that the larger momentum transfer gives larger partial cross sections. It is a little surprising that $\bar{A}_0$ for the NINA results is still

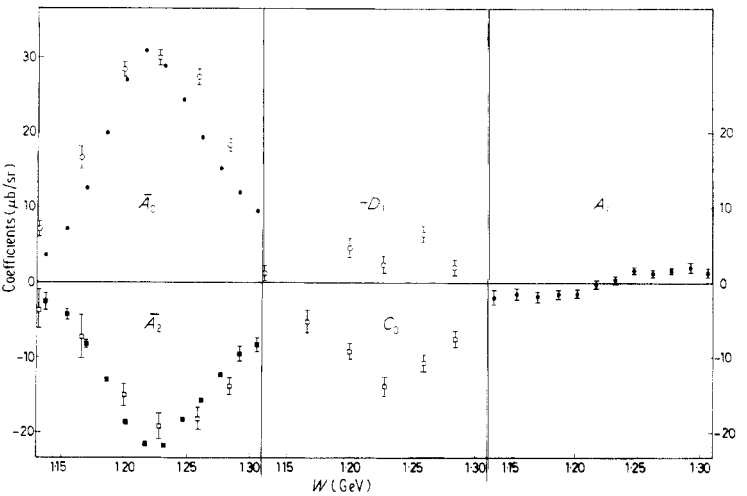

Figure 5. Coefficients of the pion angular distribution for s and p waves as functions of the π–N rest mass W for different momentum transfers q^2. Photoproduction $q^2 = 0$; CEA, $q^2 = 0{\cdot}25$ (GeV/c)^2.

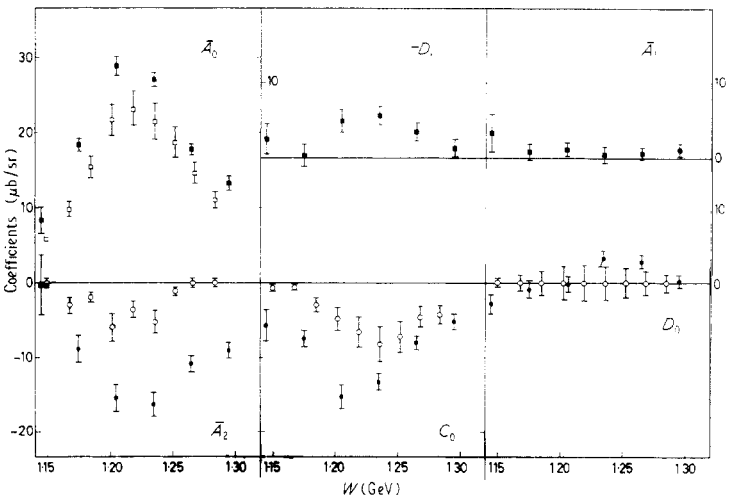

Figure 6. Coefficients of the pion angular distribution for s and p waves as functions of the π–N rest mass W for different momentum transfers q^2. Karlsruhe/DESY, $q^2 = 0{\cdot}35$ (GeV/c)^2; NINA, $q^2 = 0{\cdot}45$ (GeV/c)^2.

about 30 μb sr^{-1} at resonance as in photoproduction. Otherwise there is again a clear indication for a longitudinal–transverse interference, which most likely looks resonant. $\bar{A}_1$ is practically zero. D_0 shows some structure in accord with interference of an s wave scalar with a resonant p wave.

In figure 7 we have results from Manchester/Lancaster at $q^2 = 0{\cdot}6$ GeV^2 and results from DESY/Collège de France at $q^2 = 0{\cdot}58$ GeV^2. Now the cross section has dropped

considerably. $\bar{A}_0$ is about 20 $\mu b\,sr^{-1}$ at the resonance. We see a very nice agreement between both sets of measurements except for the D_1 term, which in our measurements is definitely different from zero. We have made many tests for this term but it was very stable. It continues the trend we had seen before.

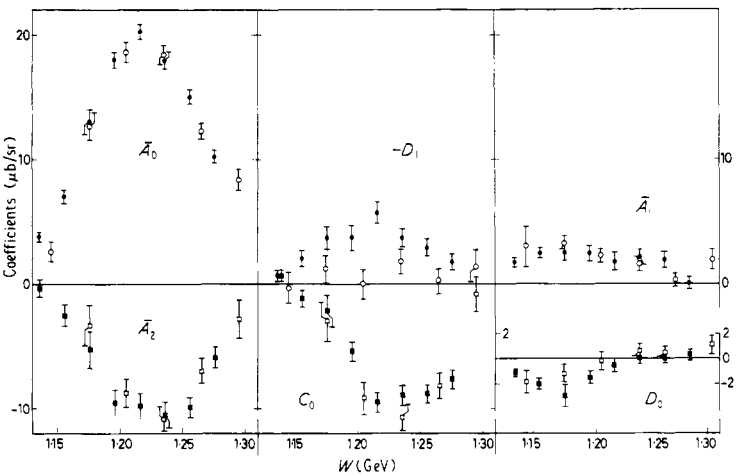

Figure 7. Coefficients of the pion angular distribution for s and p waves as functions of the π–N rest mass W for different momentum transfers q^2. ⟊ ⟊ DESY/Coll. de France, $q^2 = 0{\cdot}58$ GeV^2; ⟊ ⟊ NINA, $q^2 = 0{\cdot}6\,GeV^2$.

Finally, figure 8 shows the comparison between Karlsruhe results at $q^2 = 1{\cdot}0\,GeV^2$ and DESY/Coll. de France results at $q^2 = 0{\cdot}98\,GeV^2$. Here the agreement for $\bar{A}_0$ and $\bar{A}_2$ is quite good and less good for C_0 and D_0. D_1 and $\bar{A}_1$ are again not evaluated by the Karlsruhe group. So in all cases we have indications for deviations from pure M_{1+} transition, in the difference between $\bar{A}_2$ and C_0 and the finite size of D_1 and $\bar{A}_1$.

In figure 9 we see all results together at the resonant energy 1236 MeV as functions of q^2. There are in this figure two more results from the CEA group and two more from the Lancaster/Manchester group. Below $0{\cdot}5\,GeV^2$ the situation looks rather sad at first glance. But bearing in mind the greater difficulties connected with the experiments from CEA and from the Karlsruhe group, one might be more sure about the behaviour of the different terms.

Before going to multipole amplitudes I would like to show a comparison with theory for the coefficients, which does not depend on assumptions about multipoles for the analysis of the experimental data. In figure 10 we see the coefficients of the DESY/Coll. de France results at $q^2 = 0{\cdot}58\,GeV^2$ and the result of the theoretical dispersion calculations by von Gehlen (1969, 1970). He solves by iteration the coupled system of integral equations for the s and p wave multipoles. For this comparison the absolute value of $|M_{1+}|$ at resonance was set equal to the experimental one. One sees a rather good agreement for all terms. The pion form factor, which influences the D_1 term quite strongly, was set equal to the isovector part of the Dirac form factor F_1.

The various groups have tried to get information on the multipoles contributing to the excitation of the resonance. Since one cannot determine all, one reduces them to

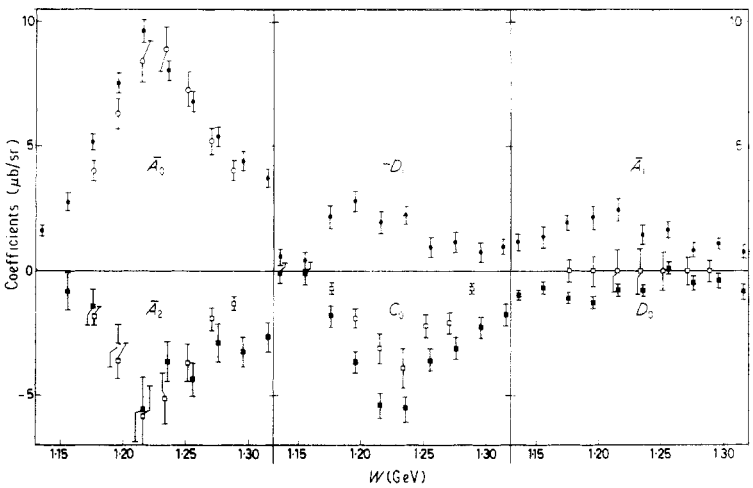

Figure 8. Coefficients of the pion angular distribution for s and p waves as functions of the π–N rest mass W for different momentum transfers q^2. Karlsruhe/DESY; DESY/Coll. de France $q^2 = 1\,(\mathrm{GeV}/c)^2$.

those combinations which might give significant contributions to the cross section. They are, besides $|M_{1+}|^2$ itself, the interferences with M_{1+}:

$$\mathrm{Re}(E_{1+}M_{1+}^*) \qquad \mathrm{Re}(S_{1+}M_{1+}^*)$$

$$\mathrm{Re}(E_{0+}M_{1+}^*) \qquad \mathrm{Re}(M_{1-}M_{1+}^*) \qquad \mathrm{Re}(S_{0+}M_{1+}^*).$$

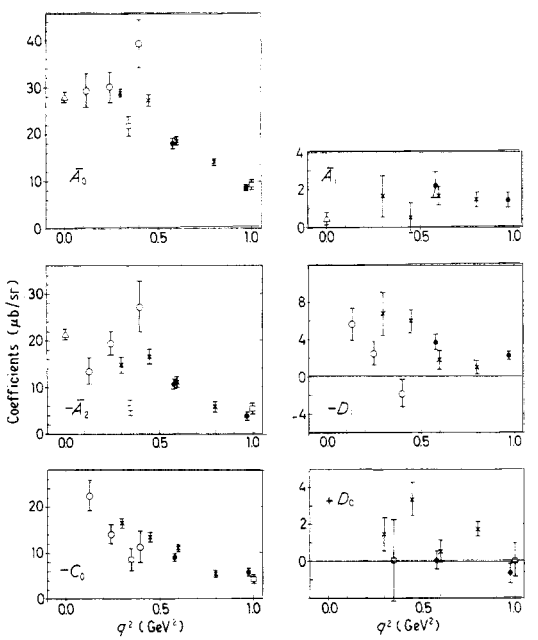

Figure 9. Coefficients of the pion angular distribution at $W \simeq 1236$ MeV as functions of the momentum transfer q^2. △ BONN (Photoproduction); ○ CEA; × NINA; □ Karlsruhe/DESY; ● DESY/Coll. de France.

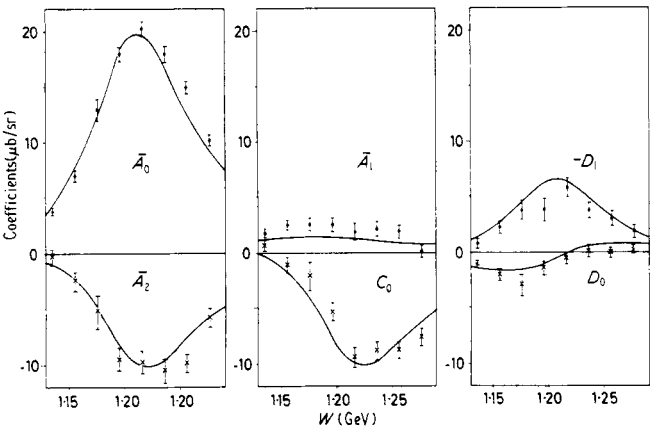

Figure 10. Coefficients of the pion angular distribution for $q^2 = 0{\cdot}58\,\mathrm{GeV}^2$, as measured by the DESY/Collège de France group (Albrecht *et al* 1970), compared with dispersion-theoretic calculations by von Gehlen (1969, 1970).

S_{1-} does not interfere with M_{1+}. All the other terms have been put to zero or other plausible assumptions have been made.

In figure 11 we see the result for one of the NINA measurements, namely for $q^2 = 0{\cdot}45\,\mathrm{GeV}^2$. They have used certain combinations of the coefficients to get just these multipole projections. The interference terms are shown in relation to $|M_{1+}|^2$, so a resonant shape is divided out. S_{1+} is at most 10 % of M_{1+} in its projection on M_{1+}, but with no significant resonance shape. E_{1+} is not significantly different from zero. E_{0+} is quite large outside the resonance as one would expect, but errors are also large. For comparison we should have a look at the corresponding quantities in photoproduction (figure 12). We have computed these values from the analysis of photoproduction data by Noelle *et al* (1970). Below resonance E_{0+} has signs different from

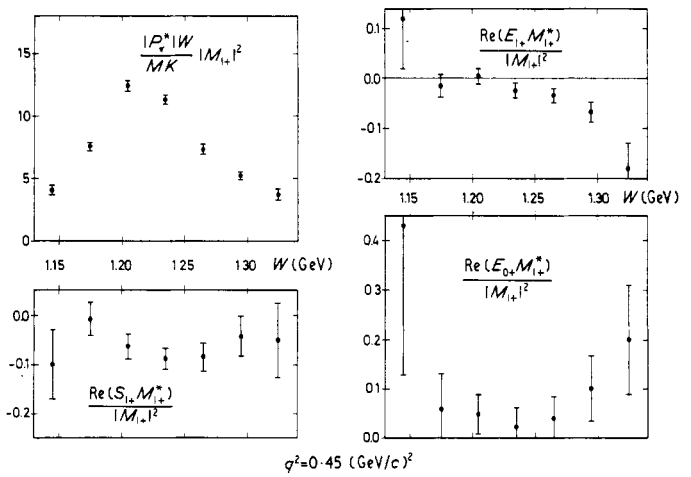

Figure 11. Multipole $|M_{1+}|^2$ and projections of other multipoles on M_{1+} for various momentum transfers as functions of the π–N rest mass.

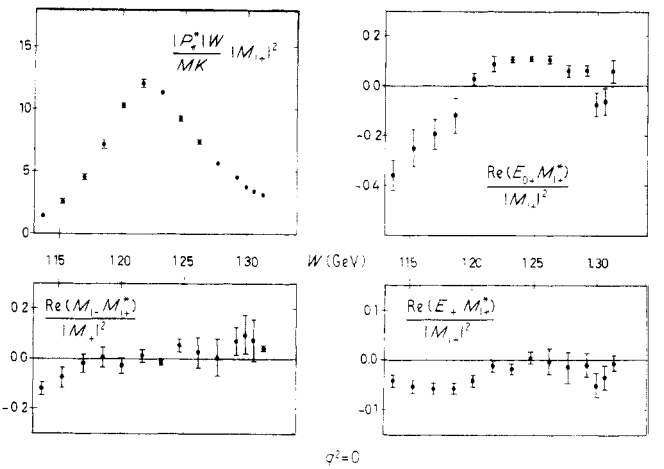

Figure 12. Multipole $|M_{1+}|^2$ and projections of other multipoles on M_{1+} for various momentum transfers as functions of the π–N rest mass.

what we saw before. At the resonance E_{0+} is larger than at $q^2 = 0{\cdot}45\ \mathrm{GeV}^2$. We have also here M_{1-}, which is not negligible far outside the resonance. In figure 13(*a*) we see an analysis of the DESY/Coll. de France measurements at $q^2 = 0{\cdot}58\ \mathrm{GeV}^2$. The S_{1+} is at most 7%. E_{1+} and M_{1-} have a similar behaviour as in photoproduction, M_{1-} going up to 30% at the lowest W value. At $q^2 = 0{\cdot}45\ \mathrm{GeV}^2$ E_{0+} has a behaviour different from that in photoproduction. The S_{0+} shows nicely the interference with the resonance, indicating that it is mostly real. The full curves are the result of calculations by von Gehlen (1969, 1970). The different multipoles show roughly the measured behaviour. One should bear in mind that the differences correspond only to a few per cent in cross section. The other two predictions are the result of Gutbrod (1969), who solves the Bethe–Salpeter equation in a ladder approximation for the resonant amplitudes, with two different assumptions for the pion form factor F_π. The agreement is again satisfactory. For absolute comparison in the calculation of Gutbrod, two cut off parameters are chosen such that at $q^2 = 0$ and at resonance the measured photoproduction values of M_{1+} and E_{1+} are reproduced. Therefore one can say that $|M_{1+}|^2$, at resonance and below, is in good agreement with the measured values, as far as the q^2 behaviour is concerned, whereas above resonance the theory gives too strong a dependence on q^2.

The multipoles for $q^2 = 0{\cdot}98\ \mathrm{GeV}^2$ from the DESY/Coll. de France experiment are shown in figure 13(*b*). The results are similar to those at $q^2 = 0{\cdot}58\ \mathrm{GeV}^2$. Figure 13(*c*) shows a comparison of those combinations of coefficients which are sensitive to $\mathrm{Re}(M_{1+}^* M_{1-})$ and $\mathrm{Re}(E_{0+}M_{1+}^*)$, for the different measurements of the Manchester/Lancaster group. The main result is that these contributions stay about the same in absolute value, while q^2 increases and the cross section decreases.

From $|M_{1+}|^2$ it is possible to calculate the γNN* transition form factor G_M^* according to

$$G_M^{*2} = |M_{1+}|^2 \frac{3\Gamma}{\alpha \sin^2\delta} \frac{(W^2 - M^2)W}{|\boldsymbol{q}|^2}$$

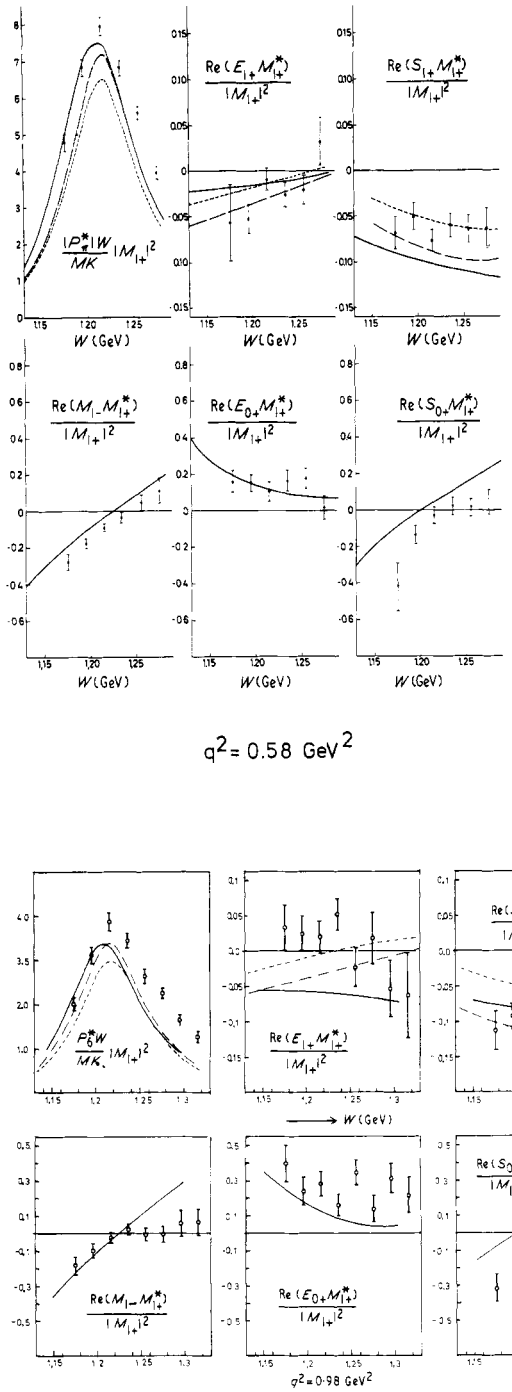

Figure 13(*a*), (*b*). Multipole $|M_{1+}|^2$ and projections of other multipoles on M_{1+} for various momentum transfers as functions of the π–N rest mass. Also shown for $q^2 = 0{\cdot}58$ GeV^2 and $0{\cdot}98$ GeV^2 are results of the dispersion-theoretic calculations by von Gehlen (1969, 1970) and by Gutbrod (1969). (– – – – – for $F_\pi = G_E^p$; ——— for $F_\pi = 1/(1+q^2/m_\rho^2)$).

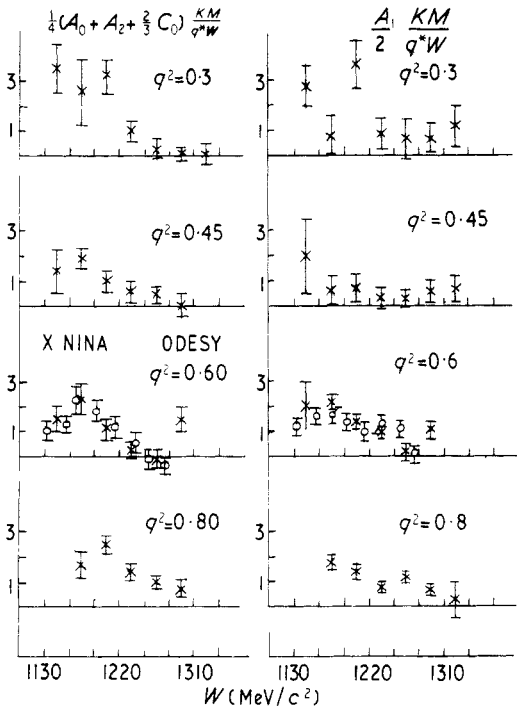

Figure 13(*c*). Coefficient combinations, which are sensitive to M_{1-} and E_{0+}, for the measurements of the Manchester/Lancaster group (Hellings *et al* 1971).

with pion–nucleon phase shift $\delta = \delta_{33}$. This is shown in figure 14(*a*) (where G_M^* is divided by $G_M^*(0) = 3$ and the dipole nucleon form factor $G_D(q^2)$), together with results from single arm measurements. For single arm measurements one fits the total cross

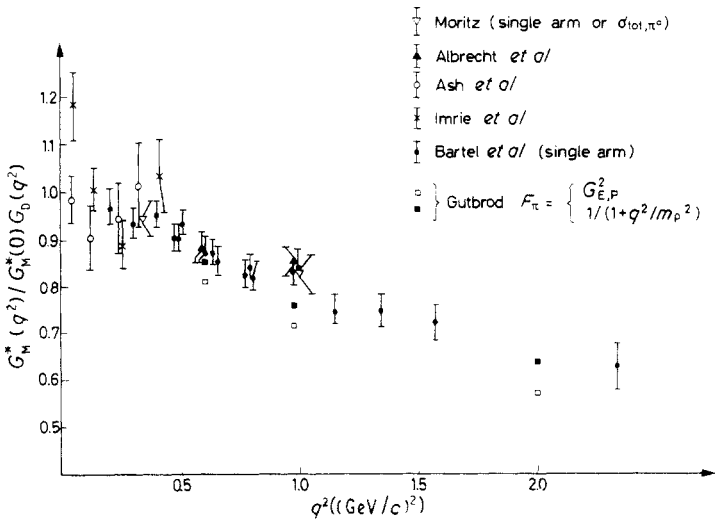

Figure 14(*a*). The γNN* form-factor as a function of the momentum transfer q^2.

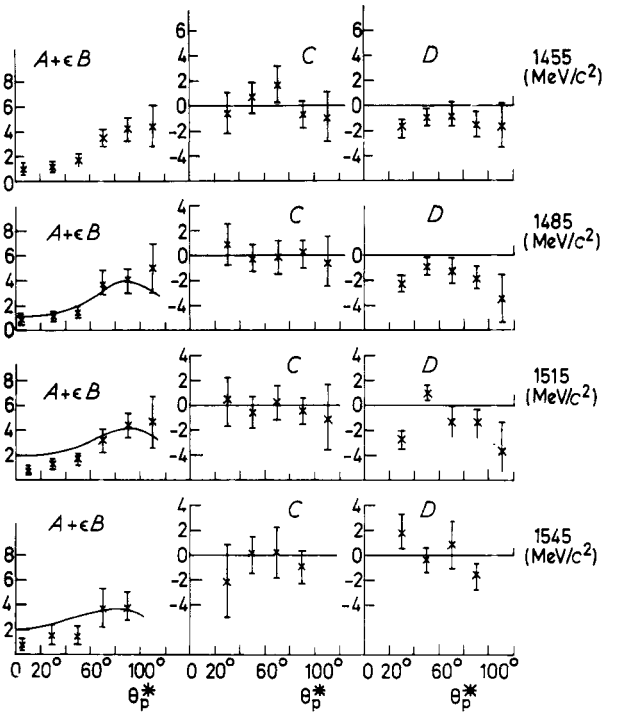

Figure 14(*b*). Measurement of pion angular distribution in second resonance region (W. J. Shuttleworth—report to this conference). The coefficients shown are $A+\epsilon B$, C, D of the expansion:

$$\frac{d\sigma}{d\Omega} = A + \epsilon B + \epsilon C \sin^2\theta_p^* \cos 2\phi_p + \{\epsilon(1+\epsilon)\}^{1/2} D \sin\theta_p^* \cos\phi_p.$$

The full lines show the corresponding measurements of A for real photons (where $B = 0$).

section across the resonance by a resonant part

$$\sigma_{res}(W, q^2) = \frac{\pi\alpha|\boldsymbol{q}|^2}{2KWM} \frac{\Gamma(W)}{(W - M^*)^2 + \frac{1}{4}\Gamma^2(W)} G_M^{*2}(q^2)$$

with a nonresonant background

$$\sigma_{nonres}(W, q^2) = (W - W_s)^{1/2} \sum_{n=0}^{N} A_n(q^2)(W - W_s)^n$$

plus a tail from the second resonance calculated from the Breit–Wigner formula†. We see at $q^2 = 0{\cdot}6$ and 1 GeV^2 good agreement between both methods. For $q^2 < 0{\cdot}5$ GeV^2 it is less satisfactory. The points from Karlsruhe come from the total π^0 cross section, measured in coincidence, and which agree with the values obtained from their single arm rates where π^+ is included. Also shown is the result of Gutbrod's model. At $q^2 = 1$ GeV^2 the agreement is less good than at 0·6 GeV^2.

2.3. Coincidence measurements at the second resonance

For the *higher resonances* work on *coincidence measurements* has just started. The recent results from the Manchester/Lancaster group (Shuttleworth 1971, report to this

† $\Gamma(W)$ is the variable width.

conference) for electroproduction of π^0 at the second resonance, as shown in figure 14(*b*). The main features are that $A+\epsilon B$ has strong θ^* dependence and that C is small. To give an interpretation in terms of multipoles will be much more difficult, but it will be very interesting to see whether the ratio $|E_{2-}|/|M_{2-}|$ has changed considerably compared with photoproduction.

2.4. σ_L/σ_T below $W = 2$ GeV

There is some new information about the ratio σ_L/σ_T in the region of the higher resonances (Brasse *et al* 1971). As I said before, to do this separation one needs measurements at the same values of q^2 and W, but for different polarization ϵ. These sets of measurements do not exist. But there is a lot of data from various laboratories across the whole resonance region for values of ϵ close to unity as well as for intermediate and small values. We have therefore tried to fit most of these data as functions of $|\boldsymbol{q}|^2$ in small steps of W across the whole resonance region for two groups of them:

(i) with $\epsilon \geqslant 0{\cdot}9$

(ii) with $\epsilon \leqslant 0{\cdot}6$.

For the fitting we have used the following equation

$$\ln\left(\frac{\Sigma}{G_D^2}\right) = a(W) + b(W)\ln\left(\frac{|\boldsymbol{q}|}{\nu}\right) + c(W)\left\{\ln\left(\frac{|\boldsymbol{q}|}{\nu}\right)\right\}^3$$

where G_D is the dipole form factor and a, b and c are fitted.

This form is equivalent to the threshold behaviour for small values of $|\boldsymbol{q}|$. Neglecting c, one gets by exponentiation

$$\Sigma = G_D^2 a'(W)|\boldsymbol{q}|^b.$$

Calculating cross sections for the two cases $\epsilon \geqslant 0{\cdot}9$ and $\epsilon \leqslant 0{\cdot}6$ one can compare them for equal values of W and q^2.

The averaged values of ϵ in the two cases are approximately 0·45 and 0·95. Thus a difference between the two sets would be approximately equal to $\frac{1}{2}\sigma_L$. Figure 15 shows

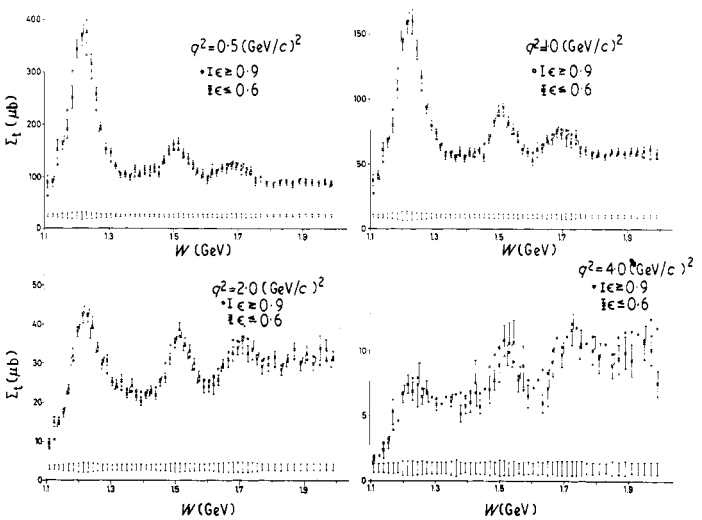

Figure 15. The total cross section Σ_t for two ranges of the polarization ϵ as calculated from fits (Brasse *et al* 1971) to all measured cross sections.

the comparison of the complete spectra for four different values of q^2. The error bars for the points with $\epsilon \geqslant 0{\cdot}9$ are put below. We could not see any significant difference between the two sets outside the error bars. Taking into account the errors, we can put the following upper limits on $R = \sigma_L/\sigma_T$:

$$\left.\begin{aligned} R &\leqslant 0{\cdot}2 \text{ for } 0{\cdot}5 \leqslant q^2 \leqslant 2{\cdot}0\,\text{GeV}^2 \\ R &\leqslant 0{\cdot}35 \text{ for } 2 \leqslant q^2 \leqslant 4\,\text{GeV}^2 \end{aligned}\right\} \text{for all } W < 2\,\text{GeV}.$$

Below 0·5 and above 4 GeV^2 there are not enough data to draw conclusions like this. It is interesting to see that R is of the same size as it is in the deep inelastic region. This may be a success of local duality.

3. Deep inelastic region

3.1. Proton and π^+ momentum spectra in the forward direction

I want now to leave the resonance region. The well known results of total cross section measurements in the *deep inelastic region* have started great activity not only among theoreticians inventing models but also among experimentalists. Coincidence measurements have to be made to get more insight into the production mechanism. Very preliminary results have been reported already at the Kiev conference by Berkelman from Cornell (Andrews *et al* 1971a, 1971b) and Pipkin from Harvard (Brown *et al* 1971a, 1971b). At this conference we have seen results from the Manchester/Lancaster group at NINA to which I will come back later. Similar experiments have been made at DESY about which I will report now.

In one of these experiments (Brasse *et al* 1971), which was carried out by my colleagues and myself, we measured the momentum spectrum of protons and π^+ mesons produced in the very forward direction with respect to the virtual photon. The reactions were the following:

$$e + p \rightarrow e + p + M_x$$

and

$$e + p \rightarrow e + \pi^+ + M_y.$$

Electrons and protons or electrons and pions were detected in coincidence and both particles were determined in all parameters, so as to be able to calculate the missing mass. The spectra were measured for the following fixed parameters of the electron:

$$\begin{aligned} E &= 6{\cdot}5\,\text{GeV} & W &= 2{\cdot}63\,\text{GeV} \\ E' &= 2{\cdot}64\,\text{GeV} & \omega &= 6 \\ q^2 &= 1{\cdot}15\,\text{GeV}^2 & \epsilon &= 0{\cdot}7 \\ |\boldsymbol{q}| &= 4{\cdot}0\,\text{GeV} & K &= 3{\cdot}2. \end{aligned}$$

These were chosen such that one is in the scaling region and on the top of the curve νW_2 against ω.

The apparatus we used is shown in figure 16. The external electron beam hits a 9 cm H_2 target and goes to a Faraday cup. The scattered electrons are measured in a double focusing magnetic spectrometer with vertical bending for the momentum

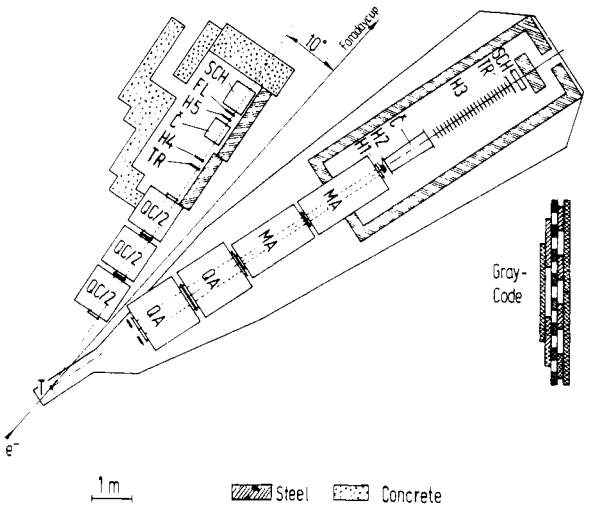

Figure 16. The apparatus used by Brasse *et al* (1971) for coincidence measurements in the deep inelastic region. H1 Hodoscope for vertical angle; H2 hodoscope for horizontal angle; H3 hodoscope for momentum; H4 and H5 hodoscope for angle and momentum; SCH showercounter; FL time of flight counter; Č Cerenkov counter; TR trigger counter.

dispersion. Scintillation hodoscopes determine momentum and angles, while Čerenkov and shower counters define the electrons. The other spectrometer for the hadrons consists of three half quadrupoles powered in series such that there is focusing in the vertical plane. Momentum and angles are measured by two hodoscopes built according to a Gray code, giving a space resolution of 3 mm. Čerenkov counter and time of flight measurement serve to identify protons and π^+ mesons, while the shower counter discriminates against positrons.

Preliminary results are shown in the next figures. We have not applied radiative corrections so far. In figure 17 the spectrum of the protons

$$\frac{d^2\sigma}{d\Omega_p\, dP_p} = \frac{1}{\Gamma}\frac{d^4\sigma}{d\Omega_e\, dE'\, d\Omega_p\, dP_p}$$

is shown against the laboratory momentum. Also shown is the scale of the centre-of-mass system (CMS) momentum. Our result is compared with photoproduction at about the same value of $W = 2{\cdot}5$ GeV, where the data are from a SLAC–Berkeley–Tufts bubble chamber collaboration (G. Wolf, private communication) selected also for the forward direction. Two things are remarkable:

(i) At high momenta the cross section is small. This is in contradiction to expectations from the field-theoretical parton model of Drell *et al* (1969a, b), where one expects that for a large part of the total cross section a fast proton comes in the direction of the virtual photon. This complete spectrum contains in the electroproduction case about 1‰ of the total cross section. Assuming a transverse momentum cut off of about 400 MeV and that, for 50% of the total cross section a proton with the longitudinal component larger than 2 GeV comes out, we should see at least 0·4% of the total cross section above 2 GeV. The experimentally found value is 0·04%.

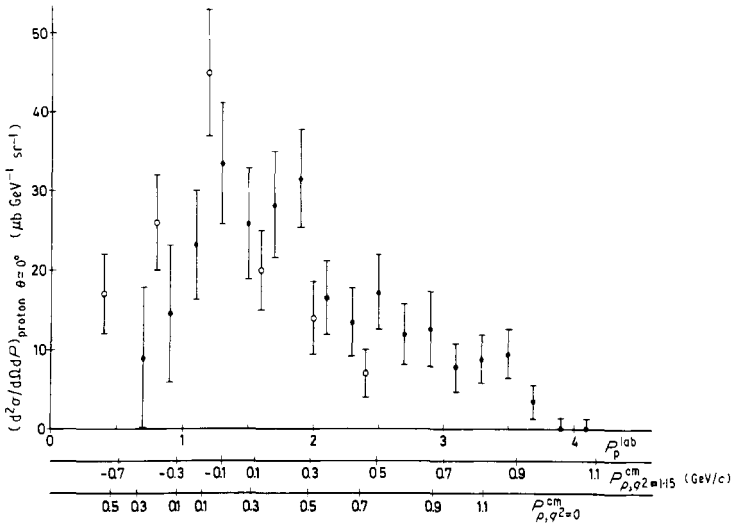

Figure 17. Proton momentum spectrum in deep inelastic electroproduction (Brasse *et al* 1971) compared with photoproduction (G. Wolf, private communication). ∤ This report, $q^2 = 1{\cdot}15$ (GeV/c)^2, $W = 2{\cdot}6$ GeV; ∤ Photoproduction, $W = 2{\cdot}5$ GeV.

(ii) However, comparing with photoproduction and taking into account that

$$\sigma_{\text{tot},q^2=0}/\sigma_{\text{tot},q^2=1\cdot15} = 3{\cdot}4$$

and also that the ratio of the Lorentz factors for the two different cases is

$$\gamma_{q^2=1\cdot15}/\gamma_{q^2=0} = 1{\cdot}5$$

then since the cross sections are about equal one comes to the conclusion that at $q^2 = 1{\cdot}15$ we have more protons in the forward direction than at $q^2 = 0$.

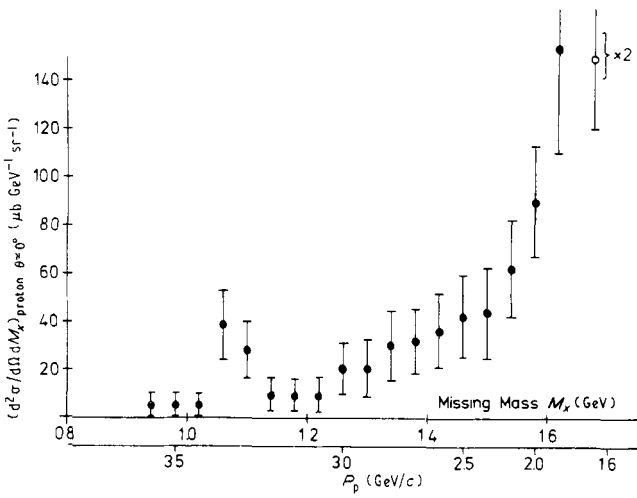

Figure 18. Missing mass distribution corresponding to the proton momentum spectrum in figure 17 with $p^{CM} > 0$.

Figure 18 shows the same protons as a missing mass spectrum. Below 1 GeV there were no events. Single π, η, ρ backward production is very small. The steep increase at the highest missing mass is mainly due to CMS–laboratory transformation. The little peak we believe to be due to the fact that we did not separate K mesons from protons and that we see here Λ or Σ electroproduction. Recalculation of the missing mass agrees with this.

In figure 19 we have the momentum spectrum of the pions also compared with the corresponding one from photoproduction. Here the number of pions is less for the same range of CMS momentum in electroproduction than in photoproduction. Figure 20 shows the conversion of this spectrum into missing mass. One clearly sees the single π^+ production and perhaps the Δ^0. Across the other resonances the cross section is rather flat and goes up only at the highest missing mass values, again as a consequence of CMS–laboratory transformations.

For a different set of kinematics, namely at

$$q^2 = 1{\cdot}6\ \text{GeV}^2$$

and

$$W = 2{\cdot}2\ \text{GeV}$$

we have also tried to get some information on the ρ electroproduction in the forward direction by detecting the recoil proton for the missing mass range of the ρ, when it is produced forward. It turned out that this is very difficult because of the low momentum of the proton and because of a very high random rate between the two spectrometers. From a new longer run we hope to get a value for the cross section at this high momentum transfer.

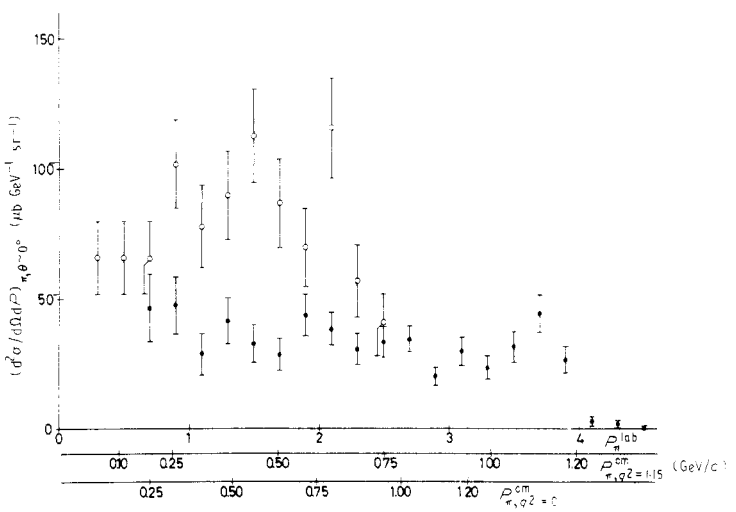

Figure 19. Pion momentum spectrum in deep inelastic electroproduction (Brasse *et al* 1971) compared with photoproduction (G. Wolf, private communication). ⁞ This report. $q^2 = 1{\cdot}15\ (\text{GeV}/c)^2$, $W = 2{\cdot}6$ GeV; ⁞ photoproduction, $W = 2{\cdot}5$ GeV.

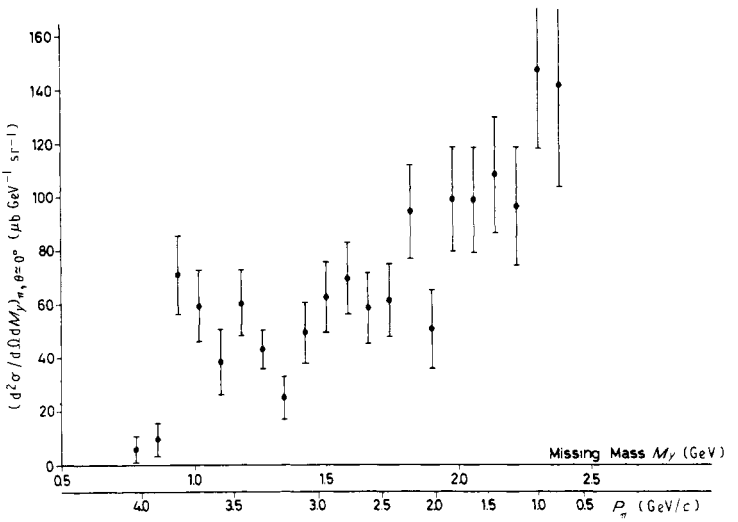

Figure 20. Missing mass distribution corresponding to the pion momentum spectrum in figure 19.

3.2. Single π^+ production on hydrogen

Finally I will discuss the very nice results of the group of Driver *et al* (1971). They have collected a large amount of data for electroproduction of specific channels such as

$$\begin{aligned} e+p &\rightarrow e+\underline{\pi}^+ + n \\ &\quad\ \underline{\pi}^+ + \Delta^0 \\ &\quad\ \underline{\pi}^+ + \pi^- + p \\ &\quad\ \underline{p} + \rho \text{ (backward)} \end{aligned}$$

in the momentum transfer range of $0{\cdot}1 \leqslant q^2 \leqslant 0{\cdot}9\ \text{GeV}^2$ and $W = 2{\cdot}2\ \text{GeV}$.

Results are available so far only for single π^+ production. The apparatus they use is shown in figure 21. The external electron beam hits a 3 cm liquid hydrogen target and goes then through a shielded pipe to a Faraday cup. Two almost identical arms measure electrons and pions or protons. Each arm consists of a bending magnet, a set of optical spark chambers, trigger counters, gas threshold Čerenkov counters to identify electrons or pions and a shower counter. The primary beam is shielded from the fringing field of the magnets by an iron pipe and the detection system against background from the beam and direct sight of the target by lead and concrete.

A typical missing mass spectrum is shown in figure 22, where one sees the single pion peak very nicely and also the first and maybe even the second resonance ($q^2 \sim 0{\cdot}4\ \text{GeV}^2$).

Before presenting their results for π^+ production, I have to introduce their notation, which is somewhat different from the one used for the resonance production. The cross section for the production by virtual photons is given by

$$\begin{aligned} \frac{d^2\sigma}{dt\,d\phi} &= \frac{1}{\Gamma'}\frac{d^4\sigma}{dE'\,d\Omega_e\,dt\,d\phi} \\ &= \sigma_u(s,q^2,t) + \epsilon\sigma_L(s,q^2,t) + \epsilon\sigma_T(s,q^2,t)\cos 2\phi \\ &\quad + \{2\epsilon(\epsilon+1)\}^{1/2}\sigma_I(s,q^2,t)\cos\phi \end{aligned}$$

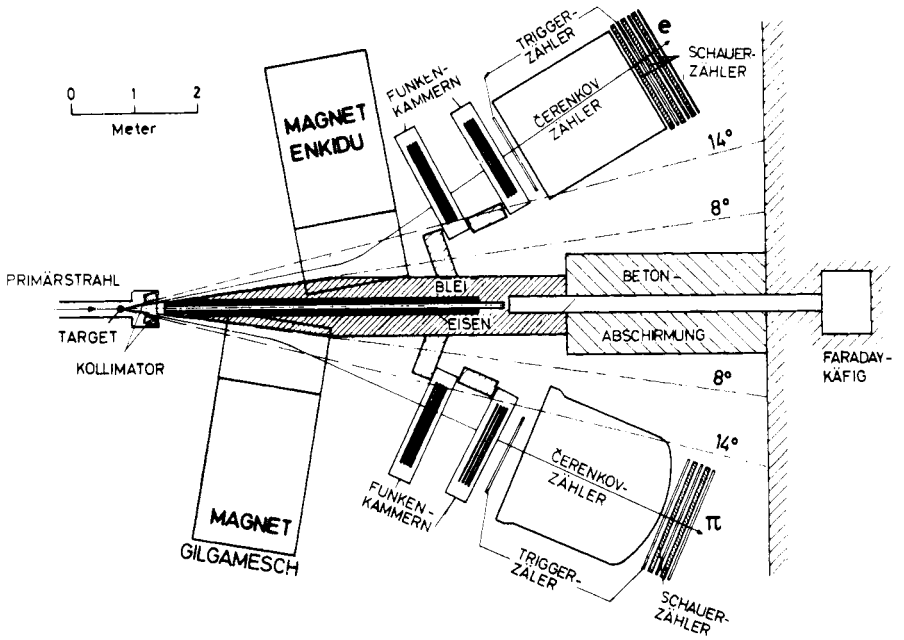

Figure 21. The apparatus used by Driver *et al* (1971) for single π^+ electroproduction.

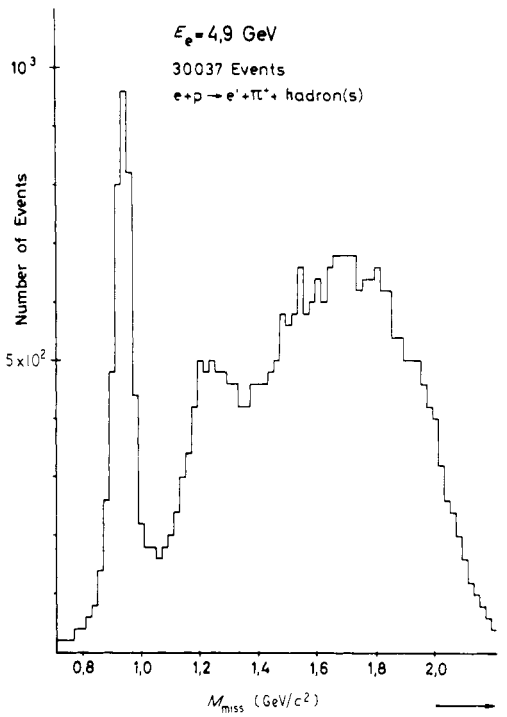

Figure 22. Typical missing mass spectrum obtained in electroproduction (Driver *et al* 1971).

where σ_u, σ_L, σ_T, σ_I correspond to the above A, B, C and D. t is the momentum transfer to the nucleon and Γ' is a kinematical factor similar to Γ.

They have not varied ϵ, so they are not able to separate directly σ_u and σ_L. Figure 23 shows their results for $t = -0{\cdot}037\,\text{GeV}^2$. $\sigma_u + \epsilon\sigma_L$, σ_T and σ_I are shown as a function of q^2. Also shown are the photoproduction values of σ_u and σ_T. The surprising result is that $\sigma_u + \epsilon\sigma_L$ increases at first as q^2 increases from 0 to $0{\cdot}4\,\text{GeV}^2$.

Also shown are results of the VDM calculation by Fraas and Schildknecht (1971). In this model the virtual photon converts first into a vector meson, which then interacts with the proton:

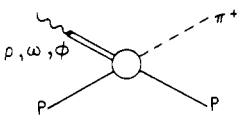

σ_u and σ_T can be written using the notations of photoproduction as

$$\sigma_u = \tfrac{1}{2}(\sigma_{\parallel} + \sigma_{\perp})$$

$$\sigma_T = \tfrac{1}{2}(\sigma_{\parallel} - \sigma_{\perp})$$

where in $\sigma_{\parallel}$ the photons are polarized in the production plane and in $\sigma_{\perp}$ they are

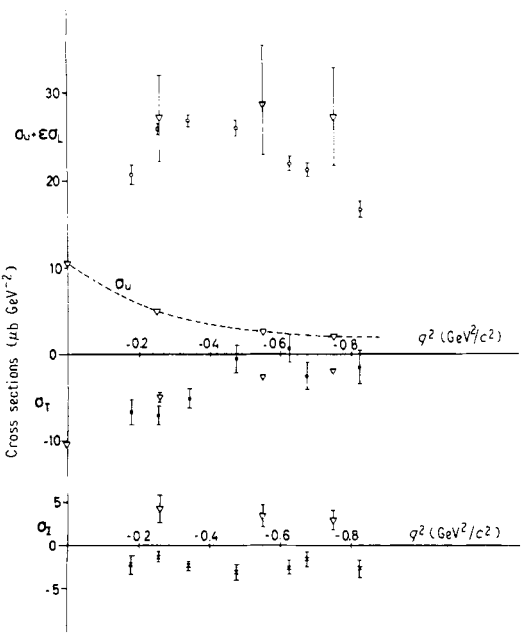

Figure 23. The cross sections: $\frac{1}{2}\sigma_U + \epsilon\sigma_L$; $\frac{1}{2}\sigma_T$ and $\frac{1}{2}\sigma_I$ as functions of q^2 for $t = 0{\cdot}037\,\text{GeV}^2/c^2$, obtained by Driver *et al* (1971). Also shown ($\dot{\gamma}$) are results of VDM calculations by Fraas and Schildknecht (1971).

polarized perpendicular to it. For these terms Fraas and Schildknecht simply have

$$\left.\begin{matrix}\sigma_{\parallel}(q^2)\\ \sigma_{\perp}(q^2)\end{matrix}\right\} = \frac{m_\rho^4}{(q^2+m_\rho^2)^2}\left\{\begin{matrix}\left(\frac{d\sigma_{\parallel}}{dt}\right)_{q^2=0}\\ \left(\frac{d\sigma_{\perp}}{dt}\right)_{q^2=0}\end{matrix}\right.$$

the ρ propagator giving the q^2 dependence (setting $m_\omega = m_\rho$ and neglecting ϕ contribution).

The longitudinal part gets an additional factor q^2/m_ρ^2 from current conservation, which makes it vanishing for $q^2 \to 0$. They deduce the following result:

$$\sigma_L = \frac{q^2}{m_\rho^2}\frac{m_\rho^4}{(q^2+m_\rho^2)^2}\frac{\rho_{00}^0}{\rho_{++}^0}\frac{1}{2}\left(\frac{d\sigma}{dt}(\gamma p \to \pi^+ n)+\frac{d\sigma}{dt}(\gamma n \to \pi^- p)\right)$$
$$+\text{interference term for } \rho, \omega.$$

Here ρ_{00}^0 and ρ_{++}^0 are the density matrix elements in the helicity frame for longitudinal and transverse ρ^0 mesons.

For the transverse–longitudinal interference the result is

$$\sigma_I = \left(\frac{q^2}{m_\rho^2}\right)^{1/2}\frac{m_\rho^4}{(q^2+m_\rho^2)^2}\frac{\mathrm{Re}\,\rho_{10}^0}{\rho_{++}^0}\frac{1}{2}\left(\frac{d\sigma}{dt}(\gamma p \to \pi^+ n)+\frac{d\sigma}{dt}(\gamma n \to \pi^- p)\right)$$
$$+\rho, \omega \text{ interference.}$$

Since ρ_{00}^0/ρ_{++}^0 is large, they get a large σ_L which increases first with q^2.

That σ_u is approximately equal to $-\sigma_T$ is a consequence of the fact that $\sigma_{\parallel} < \sigma_{\perp}$ in photoproduction for $|t| > 0{\cdot}05\ \mathrm{GeV}^2$. The interference term does not have the correct phase as measured.

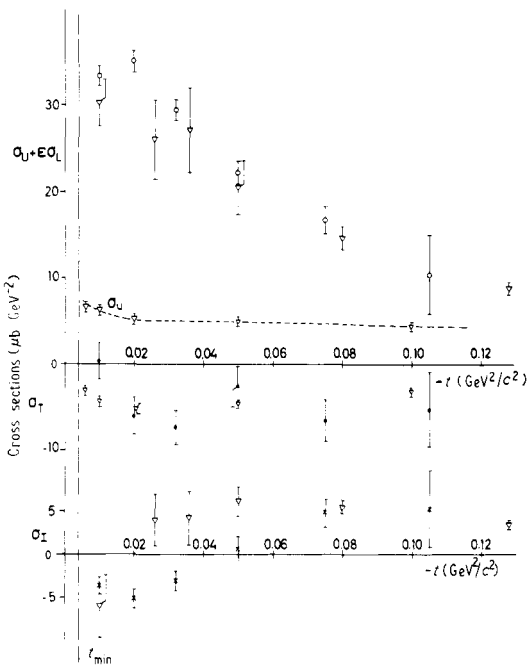

Figure 24. The t dependence of the same cross sections as in figure 23. ½ VDM predictions; $W^2 = 4{\cdot}84\ \mathrm{GeV}^2$, $q^2 = -0{\cdot}26\ (\mathrm{GeV}/c)^2$.

Figure 24 shows the t dependence for $q^2 = 0{\cdot}26\ \mathrm{GeV}^2$. The dependence of $\sigma_u + \epsilon\sigma_L$ is rather steep. σ_T and σ_l go to zero for $t \to t_{min}$, as they should. The phase between longitudinal and transverse changes sign at a t value of about $0{\cdot}05\ \mathrm{GeV}^2$.

In figure 25 we see the σ_L, which has been separated from σ_u under the assumption that the photoproduction ratio of $\sigma_{\|} \ll \sigma_{\perp}$ holds for q^2 different from zero. σ_L has a maximum at about $q^2 = m_\rho^2$. For the t dependence of σ_L the authors give e^{Bt} with $B = 15 \pm 3\ \mathrm{GeV}^2$.

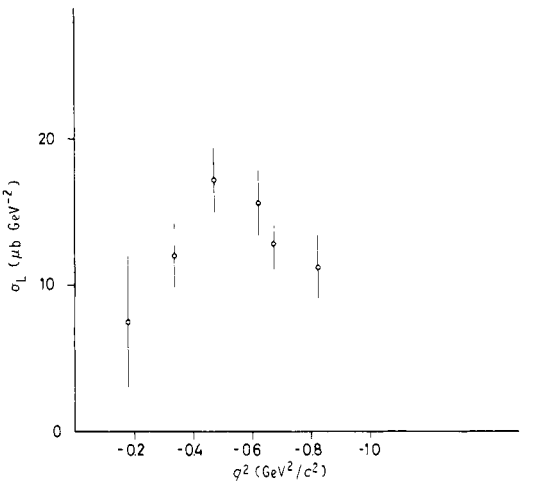

Figure 25. The longitudinal part σ_L of the cross section as found from the measurements (Driver *et al* 1971) with the assumption $\sigma_{\perp} \gg \sigma_{\|}$. $s_0 = 4{\cdot}84\ \mathrm{GeV}^2$, $t = -0{\cdot}075\ (\mathrm{GeV}/c)^2$.

In figure 26 I have compared the results of Driver *et al* with those from the Manchester/Lancaster group (Kummer *et al* 1971 and to be published). They have measured π^+ production at $q^2 = 0{\cdot}7\ \mathrm{GeV}^2$ and $W = 1{\cdot}9\ \mathrm{GeV}$. Agreement is quite good. Also shown are the results of theoretical dispersion calculations by Devenish (Devenish and Lyth 1971), indicating the strong influence of the pion form factor.

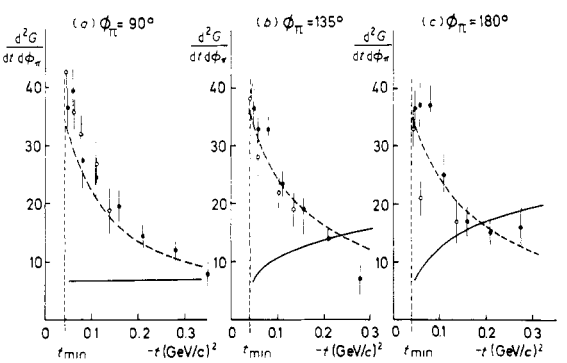

Figure 26. Results for single π^+ electroproduction of: ‡ Kummer *et al* (1971) at $q^2 = 0{\cdot}7\ \mathrm{GeV}^2$ and $W = 1{\cdot}9\ \mathrm{GeV}$ compared with those from: ◊ Driver *et al* (1971), which have been extrapolated from $W = 2{\cdot}2\ \mathrm{GeV}$ to $W = 1{\cdot}9\ \mathrm{GeV}$, and with dispersion-theoretic calculations of Devenish and Lyth (contribution to this conference). (——— $F_\pi = 0$, – – – – $F_\pi = 0{\cdot}42$).

References

Albrecht W *et al* 1970 *Nucl. Phys.* B **25** 1–8.
—— 1971 *Nucl. Phys.* B **27** 615–20.
Andrews D E *et al* 1971a *Cornell Lab. Nucl. Sci. Preprint* CLNS-136.
Andrews D E *et al* 1971b *Phys. Rev. Lett.* **26** 864–6.
Bartel W *et al* 1971 *Phys. Lett.* **35B** 181–4.
Bartel W *et al* 1968 *Phys. Lett.* **27B** 660–2.
Bätzner K *et al* 1971 *Rep. Frühjahrstagung* 1971 *des Fachausschusses Kernphysik und Hochenergiephysik* B (Hamburg: Teilchenphysik).
Brasse F W, Engler J, Ganssange E and Schneizer M 1968 *Nuovo. Cim.* **55** 679–89.
Brasse F W *et al* 1971 *Report of Deutsches Elektronen-Synchrotron* DESY 71/2.
Brasse F W *et al* 1971 *Report of Deutsches Elektronen-Synchrotron* DESY 71/19.
Brown C N *et al* 1971a *Phys. Rev. Lett.* **26** 987–90.
—— 1971b *Phys. Rev. Lett.* **26** 991–4.
Devenish R C E and Lyth D H 1972 *Phys. Rev.* D in the press.
Drell S D, Levy D J and Yan T M 1969a *Phys. Rev. Lett.* **22** 744–9.
—— 1969b *SLAC PUB* 645.
Driver C *et al* 1971 *Phys. Lett.* **35B** 77–8.
Fischer G *et al* 1970 *Nucl. Phys.* B **16** 93–101.
Fraas H and Schildknecht D 1971 *Phys. Lett.* **35B** 72–6.
von Gehlen G 1969 *Nucl. Phys.* B **9** 17–54.
—— 1970 *Nucl. Phys.* B **20** 102–24.
Gutbrod F 1969 *Report of Deutsches Elektronen-Synchrotron* DESY 69/22
Gutbrod F and Simon D 1967 *Nuovo Cim.* **51A** 602—23.
Hellings R D *et al* 1971 *Nucl. Phys.* B **32** 179–88.
Kummer P S *et al* 1971 *Lett. Nuovo Cim.* **1** 1026.
Lynch H L, Allaby J V and Ritson D M 1967 *Phys. Rev.* **164** 1635–54.
Mistretta C *et al* 1969 *Phys. Rev.* **184** 1487–507.
Moritz *et al* 1970 *Dissertation Karlsruhe.*
—— 1971 *Report of Deutsches Elektronen-Synchrotron* DESY F23-71/1.
Noelle P *et al* 1970 *Bonn University Preprint* PI 2-79.